First Monolithically Integrated Dual-Pumped Phase-Sensitive Amplifier Chip Based on a Saturated Semiconductor Optical Amplifier

Wangzhe Li,*Member, IEEE,* Mingzhi Lu, Antonio Mecozzi,*Fellow, IEEE,* Michael Vasilyev,*Senior Member,IEEE*, Shamsul Arafin, *Member, IEEE*, Danilo Dadic,Leif A. Johansson,*Member, IEEE*, and Larry A. Coldren, *Fellow, IEEE*

(*Invited Paper*)

Abstract—For the first time, a monolithically integrated photonic phase-sensitive amplification chip is fabricated and demonstrated based on an InP/InGaAsP platform. Different semiconductor optical amplifiers have been fabricated as well for characterization. On the chip, two tunable laser pumps that are coherently injection-locked, respectively, from two first-order sidebands of an externally modulated tone are generated to enable signal-degenerate dual-pumped phase-sensitive amplification in a saturated semiconductor optical amplifier. Experiments on different chips are conducted to successfully demonstrate phase-sensitive amplification with approximately 6.3 dB and 7.8 dB extinction of phase-sensitive on-chip gain. Theoretical simulations are performed and agree well with experimental results. The additive noise properties of the phase-sensitive amplification chip are also investigated.

Index Terms—Phase sensitive amplifier, semiconductor optical amplifier, photonic integrated circuit, four-wave mixing

I. INTRODUCTION

OPTICALphase-sensitive amplifiers (PSAs) have been attracting increasing attention [1,2]due to unique advantages that enable them to break the 3-dB quantum limit of the noise figure (NF)[3], as well as achieve the phase regeneration to reduce phase and time jitters in optical transmission links [4-6]. Unlike a conventional phase-insensitive amplifier (PIA) such as an erbium-doped

Wangzhe Li, Shamsul Arafin, Danilo Dadic, Leif A. Johansson and Larry A. Coldren are with the Department of Electrical and Computer Engineering, University of California, Santa Barbara, CA, 93110 (e-mail: coldren@ece.ucsb.edu).

Mingzhi Lu was with University of California, Santa Barbara; Santa Barbara; CA 93110 USA. He is now with Infinera Corporation, 140 Caspian Ct., Sunnyvale, CA 94089 USA. (email: lumz85@gmail.com)

Antonio Mecozzi is now with the Department of Physical and Chemical Sciences, University of L'Aquila, L'Aquila 67100, Italy. (e-mail: antonio.mecozzi@univaq.it).

Michael Vasilyev is with the Department of Electrical Engineering, University of Texas at Arlington, Arlington, TX 76019-0016 USA. (e-mail: vasilyev@uta.edu).

fiber amplifier (EDFA), featuring an inherent minimum NF of 3-dB [7], a PSA is capable of amplifying only one of the two quadrature phase components in a light wave signal and attenuating the other. This unique feature makes it possible in theory to realize noise free amplification, leading to a NF of 0 dB, which can find numerous applications where noise levels are critical, such as optical telecommunication, remote sensing, optical spectroscopy, LIDAR and inter-satellite communication. Various PSAs have been demonstrated by using parametric down-conversion in $\chi^{(2)}$-based nonlinear materials[8, 9], such as periodically poled $LiNbO_3$ (PPLN) waveguides and nonlinear optical loop mirrors (NOLMs) [10], or using four-wave mixing (FWM) in $\chi^{(3)}$-based nonlinear media like optical fibers [2] and unsaturated semiconductor optical amplifiers (SOAs) [11]. New CMOS-compatible platforms are also emerging [12].

Among all demonstrated PSAs so far, their implementations are based on free-space bulk-crystal system or bench-top fiber systems, which makes it difficult to use them in practical scenarios. One of the challenges in realizing a practical PSA is that at input port of the PSA the phase relationship between the pump(s) and the signal must be synchronized and stabilized. Some solutions to synchronization of the pump and signal phases have been developed via pump injection locking [13] and optical phase-locked loop [14], which usually increase the complexity of the system and make it more unsuitable for use in a real application. In addition, other issues in terms of size, weight, power consumption and coupling losses also restrict the bench-top PSA's commercial allure. In order to solve this issue, photonic integration is a promising solution and can great benefit the implementation of PSAs for practical applications. Other than some obvious advantages like small footprint, light weight, reduced coupling losses and batch fabrication economies, integrated photonic chips can inherently guarantee a stable phase relationship among signal and pumps, requiring no phase-locking mechanisms, which significantly eases the implementation and practical application of PSAs.

In this paper, based on the implementation of a PSA through a dual-pump degenerate FWM process, a chip-scale PSA using a saturated SOA as a nonlinear element and different SOAs for

characterization have been fabricated and for the first time an integrated photonic PSA chip has been experimentally demonstrated. The chip and SOAs fabrication is based on an InP/InGaAsP centered quantum well (CQW) platform. On the chip, two tunable laser pumps that are coherently injection-locked from sidebands of an external modulated light wave are obtained to realize signal-degenerate dual-pumped PSA in a highly saturated SOA. A 6.3 dB and a 7.8 dB extinction ratio of gain based on different PSA chips are realized, which both agree well with simulation results. The reduction in signal-to noise ratio is also estimated based on the measured optical spectrum of the light waves before and after the PSA.

II. PROPOSED CHIP-SCALE DUAL-PUMP PSA

Figure 1 shows the schematic of the degenerate dual pump PSA. The coherent incident light waves, which consist of two pumps and one signal, are here generated based on external modulation and then are coupled into a PSA chip. On the chip, the input light waves are split into three paths via a 1 by 3 multimode interference (MMI) coupler. Along the upper and lower paths, there are two tunable Sampled-Grating Distributed-Bragg-Reflector (SG-DBR) lasers [15], each of which is injection locked by opposite modulation side-band pumps. Please note that during external modulation the signal which is carrier would be intentionally suppressed by properly biasing the modulator so that the pumps have enough power to injection lock the two SG-DBR lasers. After being injection-locked, each SG-DBR laser which selectively amplifies the corresponding pump and suppresses the other one as well as the signal behaves as a pump laser. The signal suppression in each pump laser the due to injection locking is important because such a suppression is helpful for avoiding on-chip signal-interference-induced signal power change at the input port of the PSA, which otherwise could be misinterpreted as the result of PSA. After further being amplified by a downstream SOA, the pump is filtered by an asymmetric Mach-Zehnder interferometer (AMZI) to remove the residual signal and the noise falling in the signal's spectrum, which avoids signal interference among three paths and enables the signal to be shot-noise limited.

Along the middle path, there is a phase tuner to phase shift the signal based on carrier plasma effects; therefore, the adjustable and stable phase relationship among the signal and two pumps can be achieved for observing the PSA-based signal power variation as a function of the signal's phase. Please note that, although there are two pumps along the middle path, their powers are much smaller than those along the other two paths so that the interference of the pump waves along three paths are negligible. The light waves along three paths are combined together and split again by a 3-by-3 MMI coupler to a nonlinear-SOA (NL-SOA), a long passive waveguide (WG) as a reference port, and a tap to monitor the input light waves to the NL-SOA. The PSA occurs in the NL-SOA, and the process includes two main steps. The first step is generating new signal photons. Two pumps and a signal with a stable phase relationship are sent to a nonlinear media, in which FWM

among the light waves is able to generate new signal photos with a phase which is the sum of two pumps' phases minus the original signal phase. In the second step, interference of the generated signal with original signal modulates the amplitude of the combined electrical field of the signal. Therefore, the constructive interference amplifies the amplitude of the signal's electrical field; while the destructive interference attenuates the signal. In another word, the PSA only maximally amplifies the signal when the original signal phase is 0 or π relative to the sum of two pumps' phases (in-phase components), and maximally attenuates the signal when its phase is $\pi/2$ or $3\pi/2$ (quadrature components) to the sum of two pumps' phases. Thus, the PSA gain experiences one cycle when the phase of the incident signal goes over one π, which is different from the transmission curve of a conventional Mach–Zehnder interferometer (MZI). Such a π-periodicity of the PSA gain is important and can be used to verify the implementation of the PSA. Therefore, in our demonstration of the chip-scale PSA, the relationship between the input signal phase and the signal power after the PSA can be recoded to verify the achievement of the PSA.
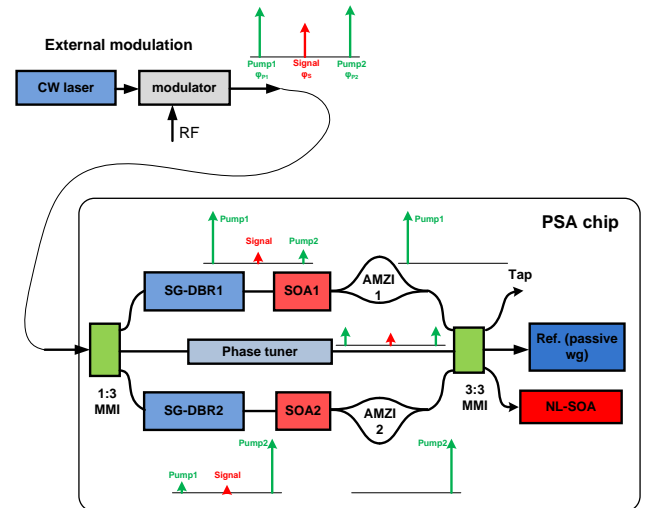

Fig. 1. Proposed schematic of demonstrating a chip scale dual-pump PSA.

One potential concern is that the SOA can be used as a PIA, and its PIA gain may interfere with the nonlinear parametric process and undermine the PSA. To overcome or minimize this issue, the incident power to the NL-SOA is high enough to saturate the NL-SOA, which is capable of suppressing the amplified spontaneous emission noise. Therefore, the saturated NL-SOA can restrict PIA and optimize the FWM [16, 17]. By recording the light wave spectrum and the signal power at the output of the NL-SOA using an optical spectrum analyzer (OSA) when changing the current applied to the phase tuner to tune the signal phase, we can evaluate the PSA performance and characterize its gain profile.

III. SOA AND PSA CHIP FABRICATION

In order to fabricate SOAs for initial characterization and monolithically integrate the single-chip dual-pumped PSA based on saturated SOA, we chose an InP/InGaAsP centered

quantum well (CQW) platform with 10 quantum wells (QWs) [18] because such a platform is capable of maximizing the mode overlap with the QWs in an SOA, enhancing the nonlinearity and maximizing the FWM.

The fabrication started with a base epi, which includes quantum well layers, waveguide layers and N-cladding layer. Active and passive areas were defined using quantum well-intermixing (QWI) technology [19]. The passive waveguide with intermixed quantum wells still confine carriers well, which is ideal for low-loss phase tuners. Then, by using electron beam lithography and methane/hydrogen/argon (MHA)-based RIE etching, the gratings of the SG-DBR laser were defined. Following the grating definition, a blanket p-cladding and p-contact layer regrowth was carried out using metalorganic chemical vapor deposition (MOCVD). After the regrowth, waveguides were defined and etched. In order to have better heat dissipation and compactness at the same time, surface ridge waveguides were used for the straight SG-DBR lasers, while more-narrow deeply-etched waveguides were used for other components on the chip, which leads to better flexibility for waveguide routing and better SOA nonlinear efficiency due to a higher confinement factor. $Cl_2/H_2/Ar$ ICP-RIE dry etching as well as InP wet etching was used to defined the features. Following the waveguide etching, P-contact vias were opened and Pt/Ti/Pt/Au was deposited as the P contact metal. To further decrease the passive waveguide loss and provide electrical isolation, we implanted protons in the p-cladding layer of the passive waveguides. The wafer was then thinned down to about 130 μm for ease of cleaving. Backside Ti/Pt/Au metallization provided common cathode connections to the n-type substrate. After cleaving and anti-reflection coating of the waveguide facets, the discrete SOAs and the PSA chips were ready for characterization. The SOAs and the chip-scale PSA were fabricated on the same wafer so that the specifications of the SOAs would be identical to those of the SOAs in the PSA chip. The length and width of the PSA chip are about 1 mm and 7 mm.
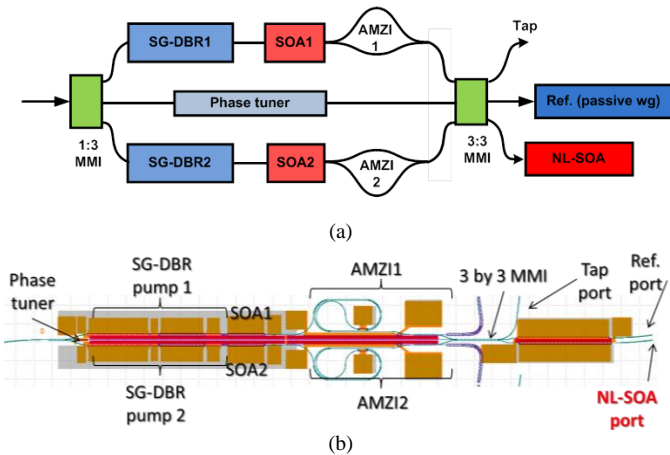

(a)

(b)

Fig. 2.(a)Schematic diagram of the PSA chip; (b)mask layout of the PSA-chip for fabrication

IV. SOA CHARACTERIZATION

Figure 3 shows all the different SOAs we fabricated. The longest SOAs are used to evaluate the dispersion. The high-speed SOAs which are the shortest are used to measure SOA's carrier lifetime; while the 1-mm SOAs are used to characterize their gain profile.
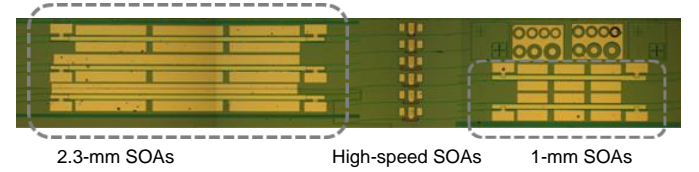

2.3-mm SOAs   High-speed SOAs   1-mm SOAs

Fig. 3.Photo of the fabricated SOAs with different lengths. (left) 2.3-mm SOAs consisting of three cascaded SOAs with a length of 766 μm; (middle) high-speed SOAs with a length of 50, 100 and 150 μm; (right) 1-mm SOAs consisting of three identical SOAs with a length of 333μm.

A. Carrier Lifetime Measurement

High-speed short SOAs were used to measure the carrier lifetime. The setup is shown in Fig. 4, which mainly includes an external cavity laser (ECL), an erbium-doped fiber amplifier (EDFA), a variable optical attenuator (VOA), a bandpass filter (BPF), a high-speed SOA, a photodetector (PD) and an electrical spectrum analyzer (ESA). A wavelength from the ECL was sent to the SOA through the EDFA, the VOA and the BPF which were used to control the input light wave power. To measure the SOA's carrier lifetime, we first measured its frequency response. To do so, an RF signal and a bias voltage were applied to the SOA via a bias-tee to modulate the light wave that was passing through the SOA. The SOA's output was converted by the PD to re-generate the RF frequency which was recorded and measured by the ESA.
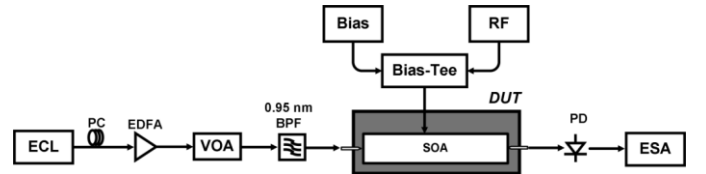

Fig. 4. SOA lifetime measurement setup

The length of the SOA under test is 50 μm, biased with a current density of 6.67 kA/cm^2. We measured SOA's frequency response given different input power, and then based on its 3-dB bandwidth, the lifetime could be calculated. We plotted the relationship between the carrier lifetime and the input power to the SOA, as shown in Fig. 5. As it can be seen, the carrier lifetime goes down to 180 μm as the input power increases to about 21 mW.
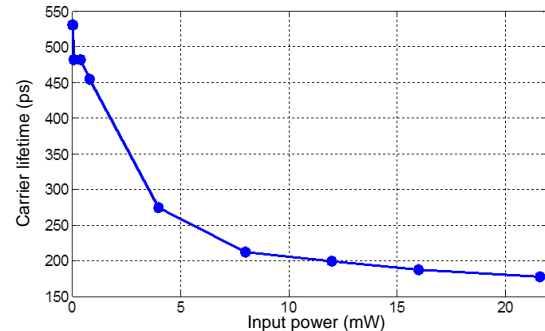

Fig. 5.Measured SOA carrier lifetime given different incident light wave power.

B. Small-Signal Gain Measurement

We took advantage of a 1-mm SOA consisting of three cascaded 333-μm SOAs to characterize its gain profile. The setup is shown in Fig. 6. Since the 1-mm SOA has three cascaded 333-μm SOAs, the first 333-μm SOA was negatively biased as a PD to measure the input power; then it was forward-biased as an amplifier to amplify the input light wave. The second 333-μm SOA was reverse-biased to detect the amplified light wave power at the output of the first 333-μm SOA.
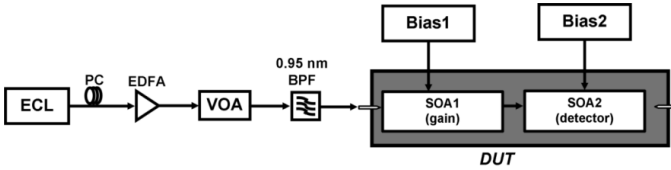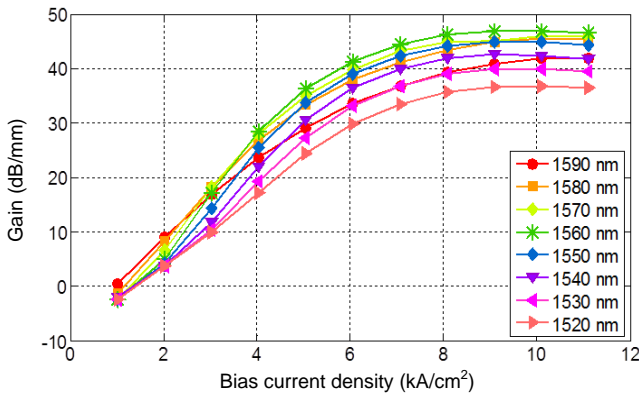

Fig. 6. SOA gain measurement setup

Fig. 7.Measured linear gain of a 1-mm SOA;

Comparing the measured input power and the power after amplification, we can obtain the gain for a 333-μm SOA. Changing the forward bias current and the input wavelength, and tripling the calculated gain, we can collect gain profiles of the 1-mm SOA, which are shown in Fig. 7. Fig. 7 shows the relationships between small-signal gain of the SOA and current density given different input wavelengths. We can see that the small-signal gain goes up as we increase the current density and becomes saturated after the current density is higher than 8 kA/cm^2. The transparent current density, given different wavelengths, is varied in the range between 1 kA/cm^2 and 1.5 kA/cm^2. Fig. 8 shows the relationship between the maximum small-signal gain and the incident wavelength when the current density is fixed. As we can see from Fig. 8, the peak small-signal gain was measured to be about 47.5 dB/mm at a wavelength of 1560 nm and a current density of 9 kA/cm^2. For the PSA experiment, we will choose a proper incident wavelength to optimize the gain of the SOAs for the operation of the PSA chip.

Because the PSA-chip is based on a saturated SOA, we need to find out the input power level to saturate the SOA. Since the length of the NL-SOA on the PSA chip is 1 mm, then we treated the 1-mm cascaded SOA as a single SOA, and we applied a current density of about 3 kA/cm^2 and measured its output power as we increased the input power. The result is plotted in

Fig. 9, showing that the 1-mm SOA would be saturated when the input power reaches about -9 dBm. Based on this input power level, we chose an incident power of 0 dB or higher to the NL-SOA on the PSA chip to ensure that the NL-SOA was deeply saturated.
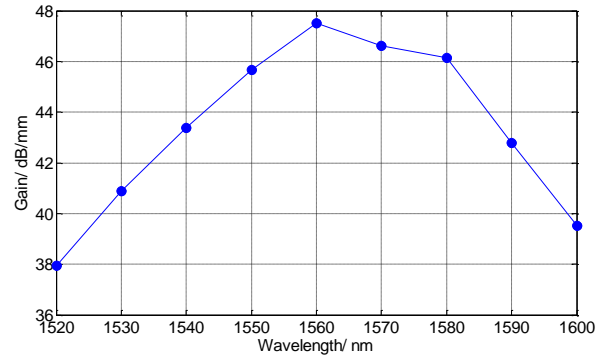

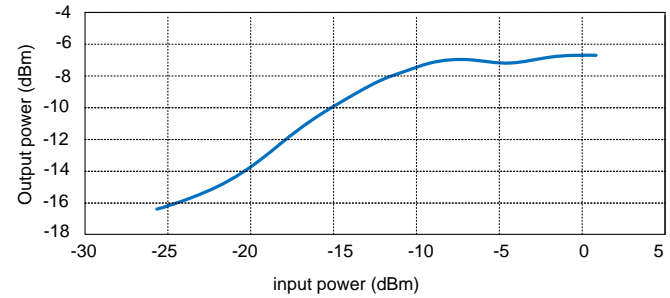Fig. 8.Measured wavelength-dependent small-signal gain profile

Fig. 9. Measured output power of the SOA with respect to the input power

C. Dispersion Measurement

In the implementation of the PSA based on a long single mode fiber or a high nonlinearity fiber, the fiber dispersion can play an important role in the PSA effect, reducing the PSA gain or gain bandwidth. Similarly, for operating the PSA chip, we have to find out the dispersion characteristics of a saturated SOA. A method to measure the dispersion has been proposed.
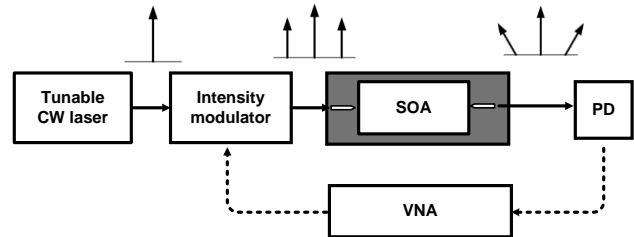

Fig. 10. SOA dispersion measurement setup

The setup shown in Fig. 10 consists of a tunable laser source, an intensity modulator (IM), a PD and a vector network analyzer (VNA). The light wave from the laser was external modulated through the IM by an RF signal applied to the IM. The RF signal was generated from the VNA. Due to the small-signal modulation, the light wave would have two more sidebands; and after passing through the SOA, nonlinear phase changes were applied to the sidebands and the original carrier due to the dispersion of the SOA. The sidebands and the carrier were sent to the PD to re-generate the RF signal which was recorded by the VNA. Then the nonlinear phase changes

introduced by the dispersion could be recovered by the comparing the RF phase changes. When we swept the input wavelength and recorded the corresponding nonlinear phase changes or the RF phase differences, we could calculate the dispersion of the SOA.
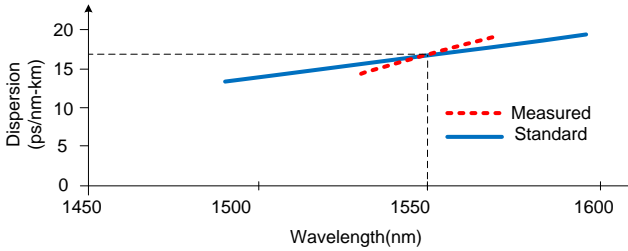

Fig. 11.Comparison of the measured dispersion of a 2-meter SMF and its standard dispersion value.

Before measuring the dispersion of the SOA, we need to evaluate this setup and prove it is functional. Therefore, we use the setup to measure the dispersion of a 2-meter signal mode fiber (SMF) and compared the result with the standard dispersion result of an ITU G.653 single mode fiber. The input wavelength was shifted from 1545 nm to 1575 nm. As we can see from Fig. 11, at 1550 nm, the measured result agrees well with the standard dispersion value; The dispersion slot is different, which could be caused by the facts that the standard SMF dispersion is based on a few km meter fiber (averaging thousands of different 2-meter SMFs) and the input wavelength was not stable and drifting during the experiment.
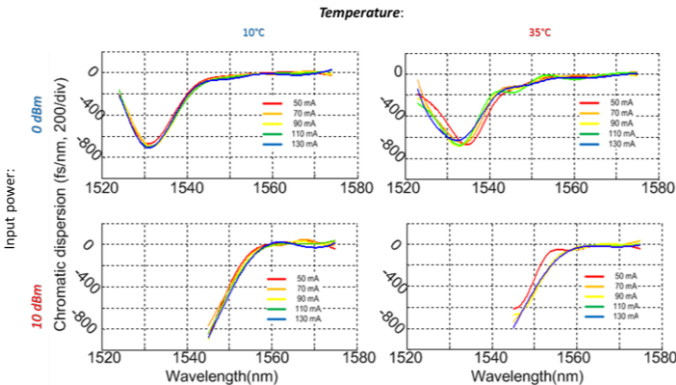

Fig. 12 Measured SOA dispersion curves given different temperatures and input powers.

After proving that the setup in Fig. 10 is functional, we measured the dispersion of a 2.3-mm SOA given different temperature and input power. The input power was set to be 0 dBm and 10 dBm, which are high enough to saturate the SOA. Please note that before each measurement, we removed the SOA first and measured the background dispersion including the modulator and the 16-meter fiber in the setup.

The measured dispersion is shown in Fig. 12, as we can see, dispersion curves are not flat. When temperature was fixed at 0 degree Celsius, given a 0-dBm input power, the dispersion is flat and close to 0 fs/nm when the wavelength falls in a range between 1550 nm to 1570 nm. At a shorter wavelength range

between 1525 nm to 1545 nm, there is a dispersion notch, and the saturated SOA shows a relatively large dispersion of -700 fs/nm, or -304 fs/nm/mm at a wavelength of 1530 nm. When the input power was increased to 10 dBm to further saturate the SOA, the measurement can only covers a wavelength range from 1545 nm to 1575 nm because of the limited gain bandwidth of the EDFA we used in the experiment; however, thanks to the appearance of the right edge of the notch, we can still tell that the dispersion curves are red-shifted. Then we increased the temperature to 35 degree Celsius, we repeated the measurement and found out that the dispersion characteristics stayed the same.

The measurement still has a few issues. The wavelength instability caused dispersion ripples on the curves; large background dispersion introduced by the 16-meter long fiber in the setup made it difficult to accurately measure the small amount of dispersion.

For the future PSA experiment and simulation, we chose the incident wavelength around 1560 nm and treated the SOA as dispersion-free element.

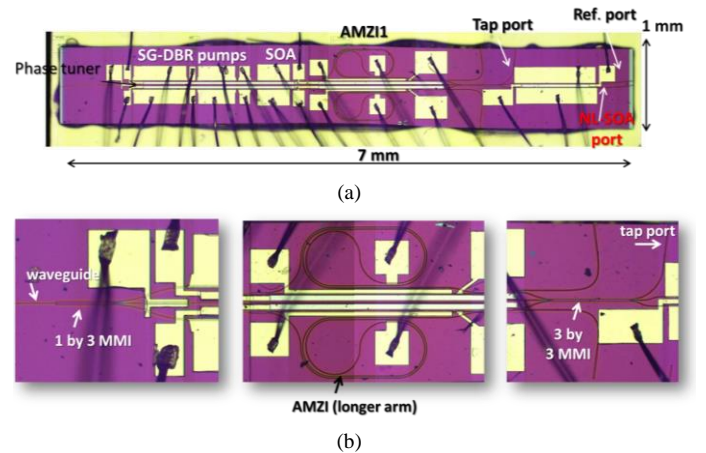## V. PSA CHIP CHARACTERIZATION

(a)

(b)

Fig. 13.(a) Photo of the signal-degenerate dual-pumped PSA chip after wire-bonding; (b) close-up views of some sections of the chip.

Fig. 13 shows a microscope picture of the fabricated PSA chip after being wire-bonded and a close-up view of some sections of the chip. We can clearly see the metal contacts which are the large golden squares, the thin waveguide at the input port of the 1 by 3 MMI, the long and curled waveguide as one arm of the AMZI, and the 3 by 3 MMI before the input of the NL-SOA and tap waveguide.

Before conducting the PSA experiment, we need to characterize the chip to choose the best chips. Specifically, we evaluated the performance of the SG-DBR lasers, the injection locking of the two SG-DBR lasers and the spurious signal interference among three paths.

A. SG-DBR Lasers

First of all, the two SG-DBR lasers were pumped and light-current-voltage (LIV) curves were measured. A typical measured LIV curve is shown in Fig. 14. The green curve is the measured laser output power as we increased the pump current.

The kink on the curve represents a mode-hopping which was caused by the internal temperate and refractive index change as we changed the current. As we can see, the SG-DBR laser has a threshold of about 30 mA at a temperature of 20 degree Celsius, and a maximum output power of about 18 dBm at a bias current of 120 mA. However, when both SG-DBR lasers were turned on, the maximum output of each one was only about 12 dBm or less due to heating effect.
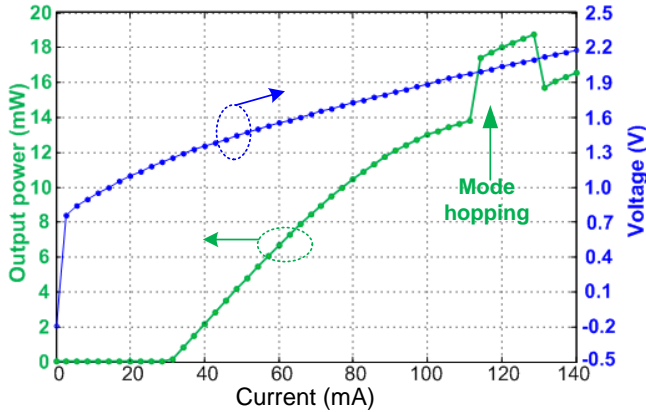

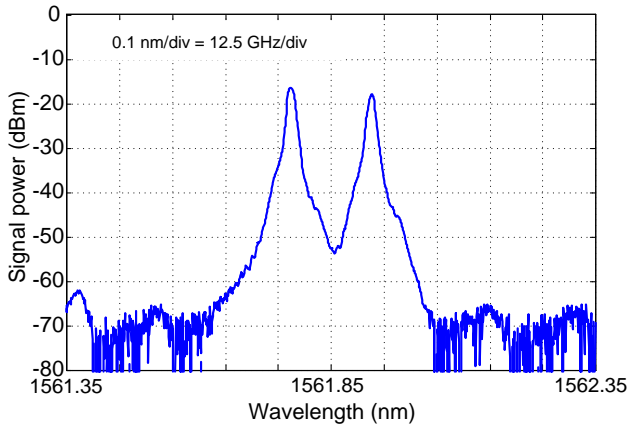Fig. 14. Measured LIV curve of a SG-DBR laser.

Fig. 15. Measured optical spectrum of the output of two free-running SG-DBR lasers.

The outputs of two SG-DBR lasers were measured as well using an optical spectrum analyzer (OSA, with a resolution of 0.01 nm) and shown in Fig. 15. The two wavelengths are spacing around 0.15 nm, which is equivalently 18.7 GHz. We can easily tune the wavelengths by changing the current applied to the corresponding phase section in each SG-DBG laser. The averaged tuning rate is about 1.18 GHz/mA. However, due to heating effect, tuning one wavelength always changed the other one in the experiment.

B. Injection Locking of Two SG-DBR Lasers

Because injection locking two SG-DBR lasers is important to make sure that the two pumps and the signal sent to the NL-SOA to have the stable phase relationship, we have to evaluate the injection locking performance of each laser.

We simply used an external laser to send the light wave to the chip and turned on only one SG-DBR laser. Then at the tap

port, we used an OSA to monitor two wavelengths and started to align them with each other. Once they were close enough, we coupled the output of the tap to an external PD to convert the light waves to an electrical beat note which was analyzed by an ESA and we observed an unstable peak due to the random phase relationship between two wavelengths. When the spacing between two wavelengths became closer and closer, we observed that the central frequency of the beat decreased. Once the two wavelengths were close enough, the beat signal disappeared and only a flat noise floor appeared on the ESA which indicated that the SG-DBR laser was injection locked and its wavelength was as same as the external one. By shifting the wavelength of the sideband through changing the frequency of the modulation RF signal, and the incident sideband power, we measured the injection locking range with respect to different injection ratio. The injection ratio is the power ratio of the incident sideband power to the laser output. Then we turned off the laser, turned on the other and repeated the same measurement. The results are plotted in Fig. 16. As we can see that the maximum locking ranges are about 4.5 GHz and 3.8 GHz when the injection ratio is maximized in the experiment. However, for the PSA experiment, both SG-DBR lasers must be injection-locked, the total input power from external modulation was distributed on two sidebands (the signal power can be ignored), which reduced the injection ratio by 3 dB. Therefore, only 3 GHz and 2.2 GHz injection locking ranges can be achieved. Considering the laser wavelength shifting due to cross heating effect when we changed the phase tuner current, the real locking range for each laser would be smaller.
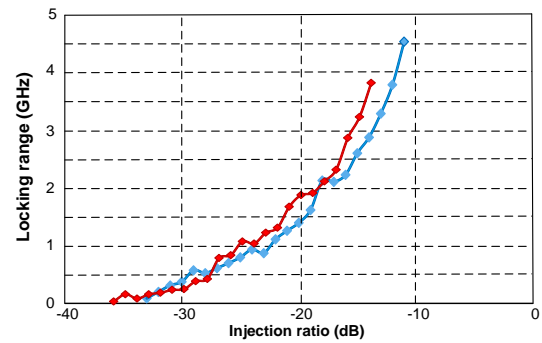

Fig. 16. Measured injection locking ranges of two SG-DBR lasers given different injection ratios.
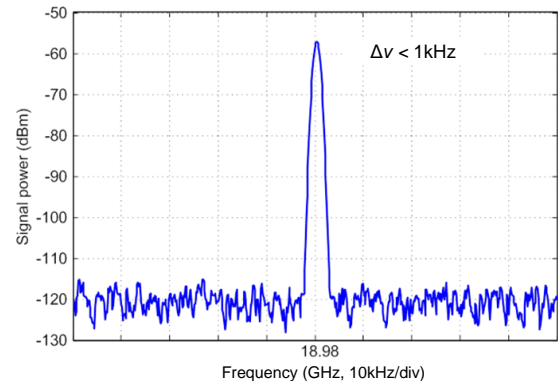

Fig. 17. Measured electrical spectrum of the beat by heterodyning the wavelengths from two injection-locked SG-DBR lasers.

Once two SG-DBR lasers were both injection- locked by the two pumps from external modulation, the beat note of two wavelengths at a PD becomes a very stable and narrow line and can be monitored by the ESA, as shown in Fig. 17. The resolution bandwidth of the ESA was about 100 Hz. The 3-dB bandwidth of the beat is less than 1 kHz, which means that once two SG-DBR lasers are injection locked, their relative frequency spacing is fixed and determined by the two pumps and their relative linewidth is also less than 1 kHz. Thus, once we obverse a stable peak with a frequency of twice the RF modulation frequency at the ESA, we can claim that the two SG-DBR lasers are injection-locked. During the PSA experiment we conducted, we always used the ESA to monitor the beat note of two SG-DBR lasers through the tap port to make ensure the injection locking was enabled.

C. Spurious Signal Interference

As we mentioned before, another advantage of injection locking is the suppression of the signal, which ensures that signal passes through the upper and middle paths, causing signal interference and leading to possible misinterpreted PSA effect. Therefore, after two SG-DBR lasers were injection-locked and before we started to evaluate the PSA by recording the signal power at the output of the NL-SOA, we have to first rule out the possibility of the signal interference among three paths to avoid improper interpretation of the PSA when shifting the signal phase by change the phase tuner current. Thus, at the output of the tap port, the signal power with respect to time and phase tuner current were measured and compared, as shown in Fig. 18. The blue solid curve is the measured signal power as we increased phase tuner current; while the dotted red curve is the measured signal power over time. By comparing two curves here, only similar random power fluctuations of about ± 0.5 dB were observed in two cases and no obvious interference among three paths was observed.

In addition, the power of the SG-DBR pump waves along the upper and the lower paths were about 15 dB higher than those along the middle path, therefore, the pump interference which could cause PSA gain drift can be ignored as well, and the signal power change at the output of the NL-SOA would be only caused by the PSA.
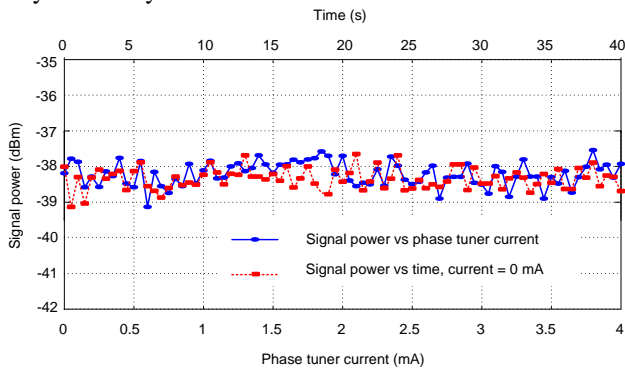

Fig. 18.Measured signal power at the output of the tap with and without phase tuner current changing.

D. Phase Tuner Characterization and Phase Shift Measurement

Tuning the phase of the signal is important for the PSA experiment. And knowing the exact phase shift when we tune the current applied to the phase tuner is more important because we need to take advantage of π-periodicity of the PSA gain curve to verify the PSA. To obtain relative phase change of the signal, we used the setup shown in Fig. 19.
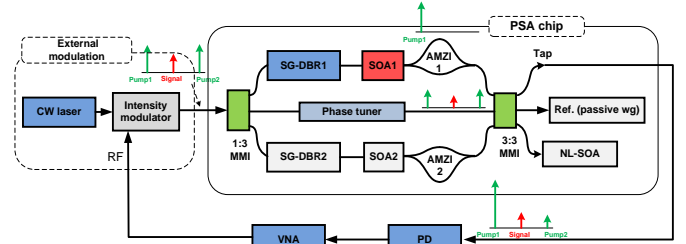

Fig. 19.Relative signal phase measurement setup.

The RF signal for the external modulation was from the VNA. One SG-DBR laser was turned off so that only one SG-DBR laser was injection locked and only one sideband was selectively amplified. Please note that the power of the amplified sideband was much larger than those of sidebands along the middle path so that the later were ignored. The signal and the amplified sideband at the output of the tap were sent to the PD to re-generate the RF signal whose phase change would be identical to that of the optical signal. Therefore, by using the VNA to measure the phase change of the received the RF signal when changing the phase tuner current, we were able to equivalently get the relative phase change of the optical signal. The result is shown in Fig. 20. The abscissa variable is set to be the square root of the phase tuner current because the signal phase in theory varies linearly with the square root of the phase tuner current. As we can see, there was no obvious phase change of the signal until after the current was larger than 1 mA. Such a delay in phase shift commonly occurs in tunable SG-DBR lasers and could be caused by an N+ sheet charge that exists at the regrowth interface due to surface contamination. As the current was further increased, these traps are filled and phase shift appeared. Overall, $1\ mA^{0.5}$ gives π phase shift of the signal.
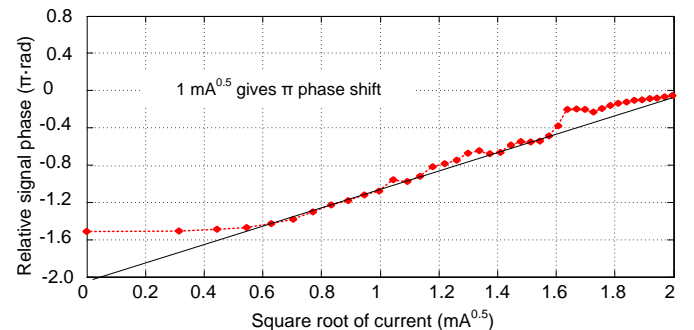

Fig. 20.Measured relative signal phase change.

To help evaluate the signal phase measurement, we also formed an on-chip MZI by deactivating the lower path. Without

external modulation, we sent one wavelength to the chip and injection locking one SG-DBR laser and measured the output power at the tap when we were changing the phase tuner current. The on-chip MZI is depicted in Fig. 21. It is well-known that the output power of the MZI varies sinusoidally with the phase difference of the light waves along two arms, and features a 2π-periodicity. Therefore, we can estimate the current-induced phase shift of the signal by observing the MZI output as we change the phase tuner current.
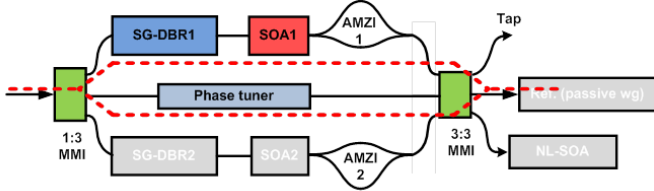

Fig. 21. On-chip MZI setup

The measured MZI output is shown in Fig. 22. As we can see, the output power barely changes when the current is less than 1 mA due to the phase delay. As the current increase, the signal power experiences one cycle. It can be clearly seen that approximately 1.1 $mA^{0.5}$ gives one π phase shift, which agrees well with the result obtained based on previous method (1 $mA^{0.5}$ gives π phase shift).
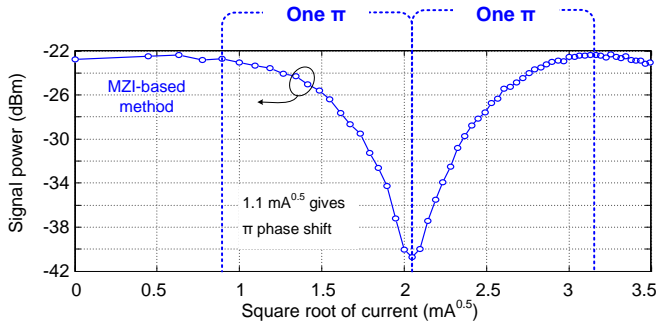

Fig. 22. Measured MZI output when changing the phase tuner current

VI. PSA EXPERIMENTAL RESULTS AND DISCUSSION

Once the basic chip characterizations were completed and the best chips were chosen, we started to configure the chip and the external modulation setup to start the PSA experiment. For external modulation, two pumps spacing about 18 GHz and one signal were generated by using an external tunable laser and an IM as in Fig. 1. The IM was properly biased to suppress the signal power, which made the sidebands' power dominant and facilitated the injection locking. The incident light waves were coupled into the PSA chip via a tapered fiber with a total coupling loss of about 6 dB. The pump power coupled into the SG-DBR laser was about -3 dBm and the output power of each laser is about 11 dBm, giving an injection ratio of about -14 dB and an injection locking ranges of 3 GHz and 2.2 GHz for two lasers, respectively. The current applied to the gain section of each SG-DBR laser fell in a range between 80 mA and 100 mA. The current to each SOA following corresponding laser lied in a range between 70 mA and 90 mA. By finely tuning the free running wavelengths of two SG-DBR lasers, the wavelength of

the external laser and the RF modulation frequency, two SG-DBR lasers could be injection locked by the two pumps. During the measurements, the wavelength of the incident signal was tuned to lie in a range between 1560 nm and 1562 nm, and the frequency of the RF signal was set to be about 9 GHz. Then the pumps and the signal were sent to the NL-SOA with a current of about 90 mA. The total input power to the NL-SOA was about -1 dBm, which was high enough to saturate the NL-SOA because the NL-SOA started saturation at -9 dBm. Once the SOA was saturated, the spontaneous emission noise and PIA were suppressed. The output of the NL-SOA was sent to the optical spectrum analyzer for recording the power of the signal as its phase was changed for PSA demonstration. The input saturation power was -9dBm. (The PIA gain is much smaller with input powers approaching the input saturation power.)
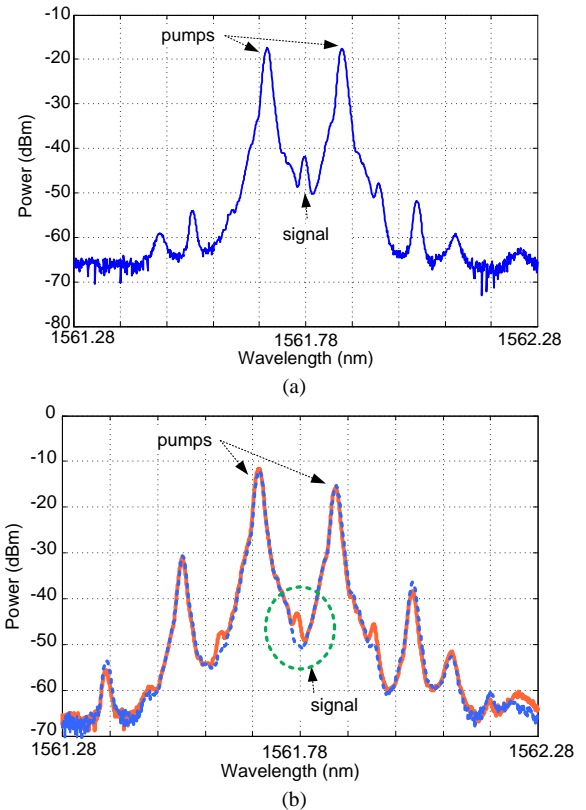

(a)

(b)

Fig. 23. Measured optical spectrum of the light wave at (a) the input and (b) the output of the NL-SOA.

The optical spectra at the input and the output of the NL-SOA were measured to record the signal power change caused by the PSA. The optical spectrum of the input light waves was equivalently obtained by monitoring the output of the tap port by using the optical spectrum analyzer. The measured optical spectra are shown in Fig. 23. Fig. 23 (a) is the optical spectrum of the input light waves. As we can see, there are two dominant pumps and one suppressed signal in the middle. Other small peaks are high-order sidebands from external modulation. Fig. 23(b) is the optical spectrum of the light wave after the PSA when the signal phase was changed by tuning the phase tuner current. Comparing with Fig. 23(a), we can clearly see the FWM and the idler waves outside the two pumps. In addition, we can see that the signal was amplified or attenuated as the

phase tuner current was adjusted. Such a current- or phase-dependent signal power change could be caused by the PSA.

To specifically demonstrate and evaluate the PSA, the measured signal power at the output of the SOA with respect to the square root of the phase tuner current was measured, which is shown in Fig. 24. Again, the abscissa variable is set to be the square root of the phase tuner current because the signal power after PSA varies with the signal phase, which is known to vary linearly with the square root of the phase tuner current. For comparison, the measured signal power without injection locking and the measured relative phase change are shown in Fig. 24 as well. As can be seen from Fig. 24, when injection locking was inactive and two lasers were in free-running modes, there was no PSA due to random phase drifting among the pumps and the signal waves. Once the injection locking was enabled, however, there was no obvious PSA or phase change of the signal until after the current was larger than 1 mA, which is caused by the phase delay we mentioned before. As the current was further increased, these traps are filled and phase-dependent signal gain appeared. Overall, 1 mA$^{0.5}$ gives π phase shift of the signal and one period oscillation of the signal. Clearly, such a signal power oscillation over one π instead of 2π phase indicates that the signal power change was caused by the PSA instead of the signal interference. The measured signal power curve shows that approximate 6.3 dB extinction of phase-sensitive on-chip gain was achieved.
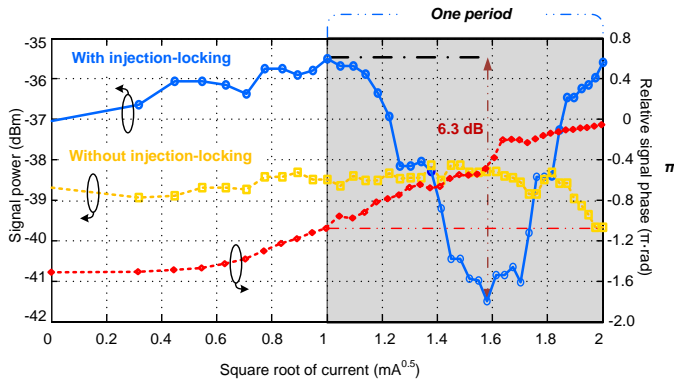

Fig. 24. Measured relationship among the signal power, the signal phase and the square root of the current applied to the phase tuner.
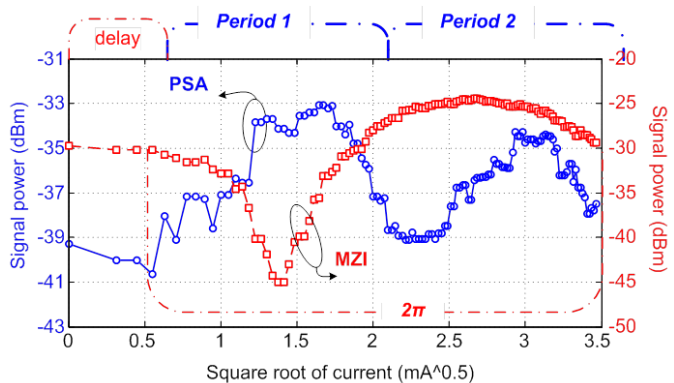

Fig. 25. Measured signal power at the output of the NL-SOA when the chip is configured as a PSA chip and the signal power at the output of the tap when the chip is configured as an MZI.

To demonstrate multiple periods of a PSA gain curve, we chose another PSA chip and repeated the same procedures but increased the phase tuner current. The results are shown in Fig. 25. The blue curve is the measured signal power change at the output of the NL-SOA caused by the PSA; while the red curve is the measured signal power at the output of the on-chip MZI. The blue curve shows a PSA gain curve of two periods, and the red curve indicates that approximately, 1.5 mA$^{0.5}$ gives one π phase shift. Amplitude reduction of the second period was probably caused by the power reduction of the input pumps as the phase tuner current was increased.
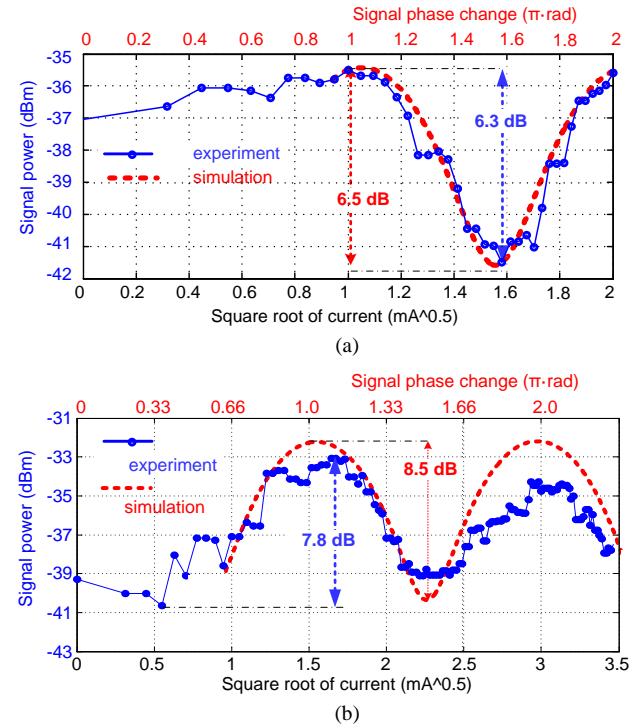

(a)

(b)

Fig. 26. Comparisons of the measured PSA gain curve and the theoretical simulation. (a) one-period PSA gain curve with 6.3 dB experimental and 6.5 dB theoretical results; (b) two-period PSA gain curve with 7.8 dB experimental and 8.5 dB theoretical results.

A theoretical simulation of the PSA gain based on coupled differential equations [17] and the model provided by Prof. Mecozzi is presented in Fig. 26(a), showing a 6.5 dB extinction ratio of the phase-sensitive gain, which agrees well with the experimental result over this current and phase-shift range. Simulation results for the second chip were obtained as well and presented in Fig. 26(b), showing a two-period PSA gain curve. Again, good agreement was observed.

The added noise of the PSA is another important aspect. Thus, the input and the output SNR of the PSA was estimated from the measured optical spectrum of light waves at the input and the output port of the NL-SOA. Please note that the input optical spectrum was equivalently measured at the output of the tap port. The signal level was the power at the signal wavelength. The noise level could not be easily measured at exactly the same wavelength, so it was measured at eight different wavelengths that were 0.5 nm away from the signal wavelength where the background spectrum was relatively flat, as shown in Fig. 27.
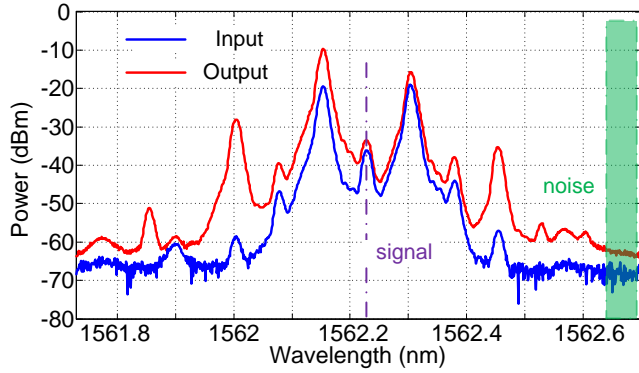
Fig. 27.The measured input and the output optical spectra of the NL-SOA.

At each wavelength, the measured SNR was obtained through 10 times iteration, as shown in Fig. 28(a), and the difference was calculated and shown in Fig. 28(b). The smallest difference in SNR was 1.5 dB and overall averaged decrease in SNR was about 2.5 dB.
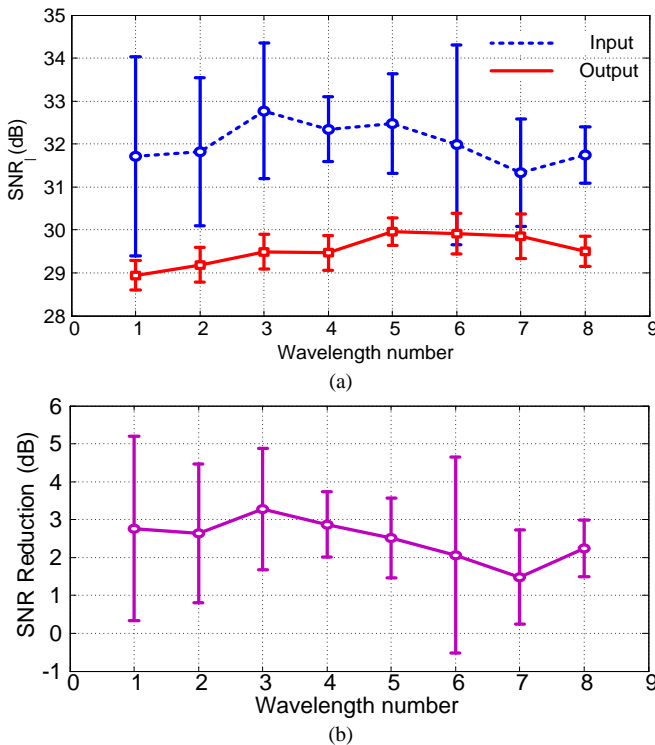

(a)

(b)

Fig. 28.(a) Measured SNR of the input and the output light waves of the NL-SOA; (b) calculated SNR reduction.

VII. CONCLUSION

Based on an InP/InGaAsP, platform we have fabricated and characterized different SOAs, and based on a highly saturated SOA, we have successfully fabricated and demonstrated the first monolithic dual-pumped PSA chip. The amplified spontaneous emission noise of the SOA was suppressed significantly due to the high saturation which restricts PIA, while high nonlinearity of the SOA benefited the PSA.

On the chip, two tunable laser pumps coherently injection-locked from sidebands of an external modulated tone were generated to enable signal-degenerate dual-pumped phase-sensitive amplification in a highly saturated semiconductor optical amplifier. Phase-sensitive amplification was experimentally achieved with approximately 6.3 dB and 7.8 dB extinction of phase-sensitive on-chip gain using two different chips. Theoretical simulations based on coupled differential equations were performed and agreed well with experimental results. The Signal-to-Noise Ratio degradation of the phase-sensitive amplification chip was also estimated, and averaged 1.5 – 3.1dB.

However, compared with high nonlinear fiber, the PSA gain is still small. The investigation of the chip-scale PSA is not comprehensive due to low current density to the NL-SOA and low incident pump power to the NL-SOA. Increasing the current density to the NL-SOA to increase the PSA gain more likely causes more heating problems, which either leads to unstable injection locking or reducing the laser pump power or possible pump interference. In addition, limited pump power to the NL-SOA restricts the saturation level of the NL-SOA, which makes it difficult to evaluate the PSA effect given a deeply saturated SOA. The PSA chip layout can be improved to allow more incident pump powers to the NL-SOA, such as using directional couplers in the PSA chip.
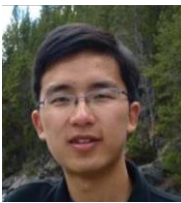
REFERENCES

[1] R. Slavík, F. Parmigiani, J. Kakande, C. Lundström, M. Sjödin, P. A. Andrekson, R. Weerasuriya, S. Sygletos, A. D. Ellis, L. Grüner-Nielsen, D. Jakobsen, S. Herstrøm, R. Phelan, J. O'Gorman, A. Bogris, D. Syvridis, S. Dasgupta, P. Petropoulos, and D. J. Richardson, "All-optical phase and amplitude regenerator for next-generation telecommunications systems," Nat. Photonics, vol. 4, no.10, pp. 690–695,2010.

[2] Z. Tong, C. Lundström, P. A. Andrekson, C. J. McKinstrie, M. Karlsson, D. J. Blessing, E. Tipsuwannakul, B. J. Puttnam, H. Toda, and L. Grüner-Nielsen, "Towards ultrasensitive optical links enabled by low-noise phase-sensitive amplifiers," Nat. Photonics, vol. 5, no. 7, pp. 430–436, 2011.

[3] C. M. Caves, "Quantum limits on noise in linear amplifiers," Phys. Rev. D., vol. 26, no. 8, pp. 1817-1839, 1982.

[4] Y. Mu and C. M. Savage, "Parametric amplifiers in phase-noise-limited optical communications," J. Opt.Soc. Am. B, vol. 9, no. 1, pp. 65-70, 1992.

[5] H. P. Yuen, "Reduction of quantum fluctuation and suppression of the Gordon-Hauseffect with phase-sensitive linear-amplifiers," Opt. Lett., vol. 17, no. 1, pp. 73-75, 1992.

[6] J. N. Kutz, W. L. Kath, R.-D. Li, and P. Kumar, "Long-distance propagation in nonlinear optical fibers byusing periodically spaced parametric amplifiers," Opt. Lett., vol. 18, no. 10, pp. 802-804, 1993.

[7] P. C. Becker, N. A. Olsson, and J. R. Simpson, Erbium doped fiber amplifiers: fundamentals and technology, Academic Press, San Diego, Calif., 1999.

[8] K. J. Lee, F. Parmigiani, S. Liu, J. Kakande, P. Petropoulos, K. Gallo, and D. J. Richardson, "Phase sensitive amplification based on quadratic cascading in a periodically poled lithium niobate waveguide," Opt. Express, vol. 17, no. 22, pp.20393–20400, 2009.

[9] T. Umeki, M. Asobe, and H. Takenouchi, "In-line phase sensitive amplifier based on PPLN waveguides," Opt. Express, vol. 21, no. 10, pp. 12077–12084, 2013.

[10] M. E. Marhic, C. H. Hsia, and J.-M. Jeong, "Optical amplification in a nonlinear fibre interferometer," Electron. Lett., vol. 27, no. 3, pp. 210-211, 1991.

[11] A. D. Ellis and S. Sygletos, "Phase sensitive signal processing using semiconductor optical amplifiers,"in OFC2013, paper OW4C.1

[12] D.J. Moss, R. Morandotti, A. L. Gaeta, and M. Lipson, "New CMOS-compatible platforms based on silicon nitride and Hydex for non-linear optics,' Nature Photonics, vol. 7, pp 597-607, Aug., 2013.

[13] A. Takada and W. Imajuku, "In-line optical phase-sensitive amplifier employing pump laser injection-locked to input signal light," Electron. Lett., vol. 34, no. 3, pp. 274-276,1998.

[14] W. Imajuku and A. Takada, "In-line optical phase-sensitive amplifier with pump light source controlled by optical phase-lock loop," J. Lightwave Technol., vol. 17, no. 4, pp. 637-646,1999.

[15] L. A. Coldren, G. A. Fish, Y. Akulova, J. S. Barton, L. Johansson, and C.W. Coldren, "Tunable semiconductor Lasers: A Tutorial," J. Lightwave Technol., vol. 22, no. 1, pp. 193–202,2004.

[16] A. D'Ottavi, F. Girardin, L. Graziani, F. Martelli, P. Spano, A. Mecozzi, S. Scotti, R. Dall'Ara, J. Eckner, and G. Guekos, "Four-wave mixing in semiconductor optical amplifiers: A practical tool for wavelength conversion," IEEE J. Sel. Topics Quantum Electron., vol. 3, no. 2, pp. 522-528, 1997.

[17] A. Mecozzi, "Analytical theory of four-wave mixing in semiconductor amplifiers," Opt. Lett., vol. 19, no. 12, pp. 892–894, 1994.

[18] J. Raring, M.Sysak, A. Pedretti, M. Dummer, E. Skogen, J. Barton, S. Denbaars, and L. Coldren, "Advanced integration schemes for high-functionality/high-performance photonic integrated circuits," in Proc. IEEE SPIE, San Jose, CA, Paper 6126-19, 2006.

[19] E. Skogen, J. Barton, S. Denbaars, and L. Coldren, "A quantum-well-intermixing process for wavelength-agile photonic integrated circuits," IEEE J. Sel. Top. Quantum Electron., vol. 8, no. 4, pp. 863–869, 2002.

Wangzhe Li received his PhD from the University of Ottawa, Canada, in 2013 working on the photonic generation of microwave and millimeter wave signals, and then joined the University of California, Santa Barbara, CA, as a postdoctoral scholar where he has been working on integrated optical phase-sensitive amplifiers.

Mingzhi Lu received his B.S. degree in electrical engineering from Southeast University, Nanjing, China in 2008, and received his M.S. and Ph.D. in Electrical and Computer Engineering from the University of California, Santa Barbara, California in 2010 and 2013. After obtaining his Ph.D., he worked at UC Santa Barbara as a postdoctoral researcher between 2013 and 2014. He is currently working at Infinera Corp. as a senior PIC development engineer. His Ph.D. and postdoctoral research is mainly focused on III-V photonic integration technology, and integrated coherent optical systems, such as integrated optical phase-locked loops, coherent LIDAR, optical synthesizer and phase-sensitive amplifiers. He is currently focusing on the next-generation larger-scale photonic integrated circuits for future communication applications.

Antonio Mecozzi is a Professor and the Director of the Department of Physical and Chemical Sciences of the University of L'Aquila, Italy, Previously, he worked for 15 years in the Optical Communication Division of Fondazione Ugo Bordoni in Rome. He was a visiting scientist of the EECS Department and the Research Laboratory of Electronics of MIT from 1991 to 1992. His areas of interest include studies on soliton transmission, laser mode-locking, nonlinear propagation in fiber, polarization mode dispersion, physics and applications of semiconductor optical amplifiers, optical amplification and noise. He holds numerous patents and over 160 publications in refereed scientific journals. Prof. Mecozzi is a Fellow of the Optical Society of America and of the IEEE.

Michael Vasilyev received the M.S. degree in Physics from Moscow Institute of Physics and Technology, Russia, in 1993, and the Ph.D. degree in Electrical Engineering from Northwestern University, Evanston, IL, in 1999 for studies of quantum properties of parametric amplifiers and solitons in optical fibers. Before joining the University of Texas at Arlington (UTA) in 2003, where he is currently a Professor of Electrical Engineering, he worked at Corning Inc. in Somerset, NJ as a Senior Research Scientist, investigating noise and nonlinearities in optical fibers as well as in Raman and erbium-doped amplifiers. Prof. M. Vasilyev's interests concentrate in experimental and theoretical nonlinear and quantum optics and nanophotonics, with applications to classical and quantum information processing, ultra-sensitive measurements, and remote sensing. He has 54 journal and over 130 conference papers, as well as 10 U.S. patents, and was a recipient of 2008 DARPA Young Faculty Award. Dr. Vasilyev has served as a chair or member of technical committees for many conferences, including IEEE Summer Topicals, CLEO, OFC, Photonics West, FiO, etc., and is an associate editor for the IEEE/OSA J. of Lightwave Technology. He is a Fellow of the OSA and a Senior Member of the IEEE Photonics and Communication Societies.

Shamsul Arafin is currently working as an Assistant Project Scientist in the University of California at Santa Barbara (USCB), USA under the supervision of Prof. Larry A. Coldren. Prior to joining UCSB, he worked as a Postdoctoral Research Scholar in Device Research Laboratory at the University of California at Los Angeles, USA. He received the B.Sc. degree in Electrical and Electronics Engineering from Bangladesh University of Engineering and Technology (BUET), Bangladesh in 2005 and the M.Sc. degree in Communication Technology from Universität Ulm, Germany, in 2008. He received his Ph.D. degree from Technische Universität München, Walter Schottky Institut Germany in 2011. In 2012, he worked at the nanophotonics group of Electrical and Computer Engineering Department at McGill University as a post-doc fellow.

Danilo Dadic received his B.S. in Physics from the University of California, Los Angeles, CA (UCLA) in 2014. He is currently working towards his M.S./PhD at the University of California, Santa Barbara, CA (UCSB) in the Electrical and Computer Engineering Department. His research focus is on the design, fabrication, and characterization of photonic integrated circuits closely integrated with electronic integrated circuits.

Leif A. Johansson (M'04) received a Ph.D. degree in engineering from University College London, London, U.K., in 2002. He has worked as a Research Scientist with the University of California, Santa Barbara since that time, and he is also a founder of Freedom Photonics where he is currently employed. His current research interests include design and characterization of integrated photonic devices for analog and digital applications and analog photonic systems and subsystems.

Larry A. Coldren (S'67–M'72–SM'77–F'82) received the Ph.D. degree in Electrical Engineering from Stanford University, Stanford, CA, in 1972. After 13 years in the research area at Bell Laboratories, he joined University of California, Santa Barbara in 1984. He is the Fred Kavli Professor of Optoelectronics and Sensors and holds appointments in the Departments of Materials and Electrical and Computer Engineering. From 2009 – 2011 he served as Dean of the College of Engineering. In 1990, he cofounded Optical Concepts, later acquired as Gore Photonics, to develop novel VCSEL technology, and, in 1998, he cofounded Agility Communications, later acquired by JDSU, to develop widely-tunable integrated transmitters.

At UCSB, he has worked on multiple-section widely-tunable lasers and efficient vertical-cavity surface-emitting lasers (VCSELs). More recently, his group has developed high-performance InP-based photonic integrated circuits (PICs) as well as high-speed VCSELs.

He has authored or coauthored over a thousand journal and conference papers, He also has co-authored eight book chapters, a widely used textbook, and has been issued 65 patents. He is a recipient of the 2004 John Tyndall, 2009 Aron Kressel, 2014 David Sarnoff, and 2015 IPRM Awards, and he is a Life Fellow of the IEEE, a Fellow of the OSA and IEE, and a member of the National Academy of Engineering.